3-D resistivity forward modeling and inversion using conjugate gradients

Jie Zhang*, Randall L. Mackie*, and Theodore R. Madden*

ABSTRACT

We have developed rapid 3-D dc resistivity forward modeling and inversion algorithms that use conjugate gradient relaxation techniques. In the forward network modeling calculation, an incomplete Cholesky decomposition for preconditioning and sparse matrix routines combine to produce a fast and efficient algorithm (approximately 2 minutes CPU time on a Sun SPARCstation 2 for 50 × 50 × 20 blocks). The side and bottom boundary conditions are scaled impedance conditions that take into account the local current flow at the boundaries as a result of any configuration of current sources.

For the inversion, conjugate gradient relaxation is used to solve the maximum likelihood inverse equations. Since conjugate gradient techniques only require the results of the sensitivity matrix A or its transpose A^T multiplying a vector, we are able to bypass the actual computation of the sensitivity matrix and the inversion of $A^T A$, thus greatly decreasing the time needed to do 3-D inversions.

We demonstrate 3-D resistivity tomographic imaging using pole-pole resistivity data collected during an experiment for a leakage monitoring system near evaporation ponds at the Mojave Generating Station in Laughlin, Nevada.

INTRODUCTION

The earth is inherently three-dimensional. The interpretation of resistivity data, however, is usually done assuming a 1-D or 2-D geometry, although 3-D interpretation is essential in many applications such as mineral and geothermal exploration and environmental surveys for hydrogeologic investigations. However, the full use of resistivity techniques in geophysics has been limited by the inability to accurately calculate anomalies as a result of 3-D features and to efficiently compute an inversion for a large 3-D model. In the recent past, substantial advances have been made in numerical modeling techniques for 2-D geologic structures. The techniques for solving a 2-D forward modeling problem include the integral equation method (Hohmann, 1975), the network method (Pelton et al., 1978; Tripp et al., 1984), the finite-element method (Coggon, 1971) and the finite-difference method (Mufti, 1976). Least-squares techniques have been successful in the applications to 2-D inversion problems (Pelton et al., 1978; Tripp et al., 1984; Shima, 1990). However, there are only a few reported studies of 3-D resistivity forward modeling and inversions. Dey and Morrison (1979) developed a 3-D forward modeling routine using finite-difference. Petrick et al. (1981) outlined a 3-D alpha-center method that involves solving for image sources representing conductivity distributions and applying a least-squares algorithm for the inversion. Park and Van (1991) developed a 3-D inversion procedure using maximum likelihood inverse theory and Dey and Morrison's (1979) finite-difference forward modeling code. However, their inversions were limited to small models because standard matrix inversion techniques were used to solve the maximum likelihood inverse equations. Li and Oldenburg (1994) also used Dey and Morrison's (1979) 3-D finite-difference algorithm in an approximate inverse procedure without calculating the 3-D sensitivity matrix and its inversion. They performed 1-D linear inversions in the wavenumber domain and obtained an approximate 3-D solution by Fourier transforming the 1-D inversion results. Ellis and Oldenburg (1994) presented another approach for solving the pole-pole 3-D resistivity inverse problem which used the conjugate gradient method to minimize a nonlinear objective function and applied the adjoint equation to compute the gradient of the objective function.

In this paper, we use a transmission-network analogy (Madden and Swift, 1969; Swift, 1971) for the 3-D forward

modeling problem, and we apply conjugate gradient relaxation to solve both the forward and inverse problems. For the forward problem calculation, conjugate gradient relaxation is used to obtain an accurate solution of the discretized network equations for dc current flow in the earth. For the inversion, conjugate gradient relaxation is used both for the forward modeling step and for finding a solution to the linearized equations of the maximum likelihood inverse problem. We also recognize that the use of conjugate gradient relaxation in the inversion allows us to bypass the actual computation of the sensitivity matrix. Our fundamental goal is to provide a compact 3-D resistivity code that works quickly and efficiently on a modern computer workstation. Results with both synthetic and real data will be presented.

FORWARD MODELING FORMULATION AND BOUNDARY CONDITIONS

The forward modeling routine will affect both the efficiency and accuracy of the 3-D inversion algorithm. Therefore, we explore the details of several different numerical techniques for solving the forward problem and also investigate the effects of the boundary conditions. The equations that govern the dc resistivity response are

$$\nabla v(x, y, z) = -\rho(x, y, z) J(x, y, z), \qquad (1)$$

$$\nabla \cdot J(x, y, z) = i(x, y, z), \qquad (2)$$

where $v(x, y, z)$ is the electric potential, $J(x, y, z)$ is the current density, $i(x, y, z)$ is the current source distribution, and $\rho(x, y, z)$ is the 3-D resistivity distribution.

Equations (1) and (2) are seen to be the transmission network equations (Madden and Swift, 1969; Swift, 1971). For a discretized earth, they can be approximated by a network of lumped impedances where the impedances are proportional to the model resistivities. Figure 1 shows a portion of the discretized 3-D resistivity distribution and its

network analog. We define voltage nodes at the top center of each medium block. With this geometry, the impedance elements R_x, R_y, and R_z can be given by

$$\frac{1}{R_x} = \frac{1}{\dfrac{\Delta x(i)\rho(i, j, k)}{\Delta y(j)\Delta z(k)} + \dfrac{\Delta x(i-1)\rho(i-1, j, k)}{\Delta y(j)\Delta z(k)}}$$

$$+ \frac{1}{\dfrac{\Delta x(i)\rho(i, j, k-1)}{\Delta y(j)\Delta z(k-1)} + \dfrac{\Delta x(i-1)\rho(i-1, j, k-1)}{\Delta y(j)\Delta z(k-1)}}, \qquad (3a)$$

$$\frac{1}{R_y} = \frac{1}{\dfrac{\Delta y(j)\rho(i, j, k)}{\Delta x(i)\Delta z(k)} + \dfrac{\Delta y(j-1)\rho(i, j-1, k)}{\Delta x(i)\Delta z(k)}}$$

$$+ \frac{1}{\dfrac{\Delta y(j)\rho(i, j, k-1)}{\Delta x(i)\Delta z(k-1)} + \dfrac{\Delta y(j-1)\rho(i, j-1, k-1)}{\Delta x(i)\Delta z(k-1)}}, \qquad (3b)$$

$$\frac{1}{R_z} = \frac{\Delta x(i)\Delta y(j)}{\Delta z(k)\rho(i, j, k)}, \qquad (3c)$$

where $\Delta x(i)$, $\Delta y(j)$, and $\Delta z(k)$ are the grid spacing in each dimension for block (i, j, k), and $\rho(i, j, k)$ is the resistivity of block (i, j, k). On the right side in Figure 1, a lumped network of $2 \times 3 \times 2$ grids is illustrated, which consists of network nodes, boundary nodes, and impedance branches between network nodes. Current sources can be placed at any network nodes, and the voltage is defined at all nodes. Kirchhoff's current law applied to the network results in a linear set of equations that can be written in matrix form as
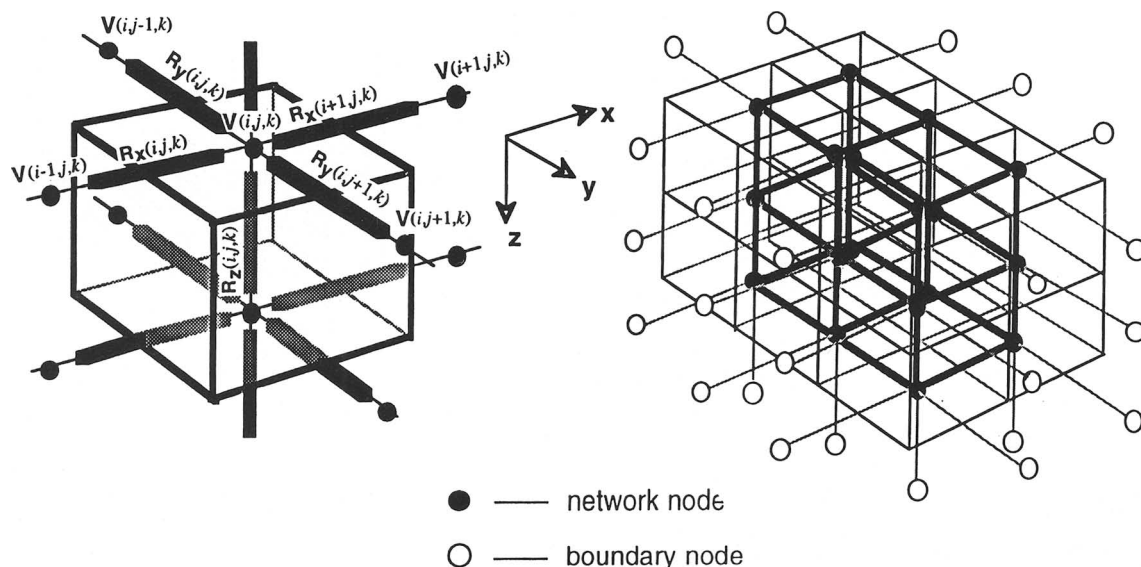

● —— network node

○ —— boundary node

FIG. 1. A portion of the discretized 3-D resistivity distribution and the resultant lumped network. R_x, R_y, and R_z represent network impedances.

$$\underline{\mathbf{K}}\boldsymbol{v} = \mathbf{s}, \tag{4}$$

where the coefficient matrix $\underline{\mathbf{K}}$ is sparse, symmetric, and positive-definite; $\boldsymbol{v}$ is the voltage vector, and $\mathbf{s}$ is the current source vector. For a model with blocks of nx, ny, and nz in three dimensions, the matrix $\underline{\mathbf{K}}$ has a size $(nx \times ny \times nz)$ by $(nx \times ny \times nz)$, and $\boldsymbol{v}$ and $\mathbf{s}$ have length $nx \times ny \times nz$.

Boundary conditions

We apply a homogeneous Neumann condition $(\partial v/\partial z = 0)$ at the earth-air interface and a scaled impedance boundary condition on the sides and bottom that is a modification of Dey and Morrison's (1979) boundary condition. In Figure 2, we illustrate a plan view of the modeling accuracy on the ground surface for four different boundary conditions that we describe below. A single pole or a dipole source with

pole-pole interval 50 m on the surface is assumed. We plot the percentage difference using the formula: $100 \times (v_a - v_{num})/v_a$, where v_a is the analytical solution and v_{num} is the numerical solution. Two models are tested: (1) homogeneous half-space ($\rho = 500 \ \Omega \cdot \mathrm{m}$) and (2) two-layer media ($\rho_1 = 500 \ \Omega \cdot \mathrm{m}$, $\rho_2 = 200 \ \Omega \cdot \mathrm{m}$, $h = 30$ m). The models ($20 \times 30 \times 15$) are gridded with equal spacing 10 m in all three dimensions.

Most of the early work in resistivity modeling used Dirichlet type of boundary conditions, where $v = 0$ is set at all boundaries except for the free surface (Mufti, 1976; Tripp et al., 1984). Using this boundary condition, one has to establish a large coarse grid system near the boundaries simply for maintaining accuracy in a small central area. Additional computer storage is then required, and the number of grids that can be modeled is limited. The error for an equally gridded model, as shown in Figure 2, can be tremen-
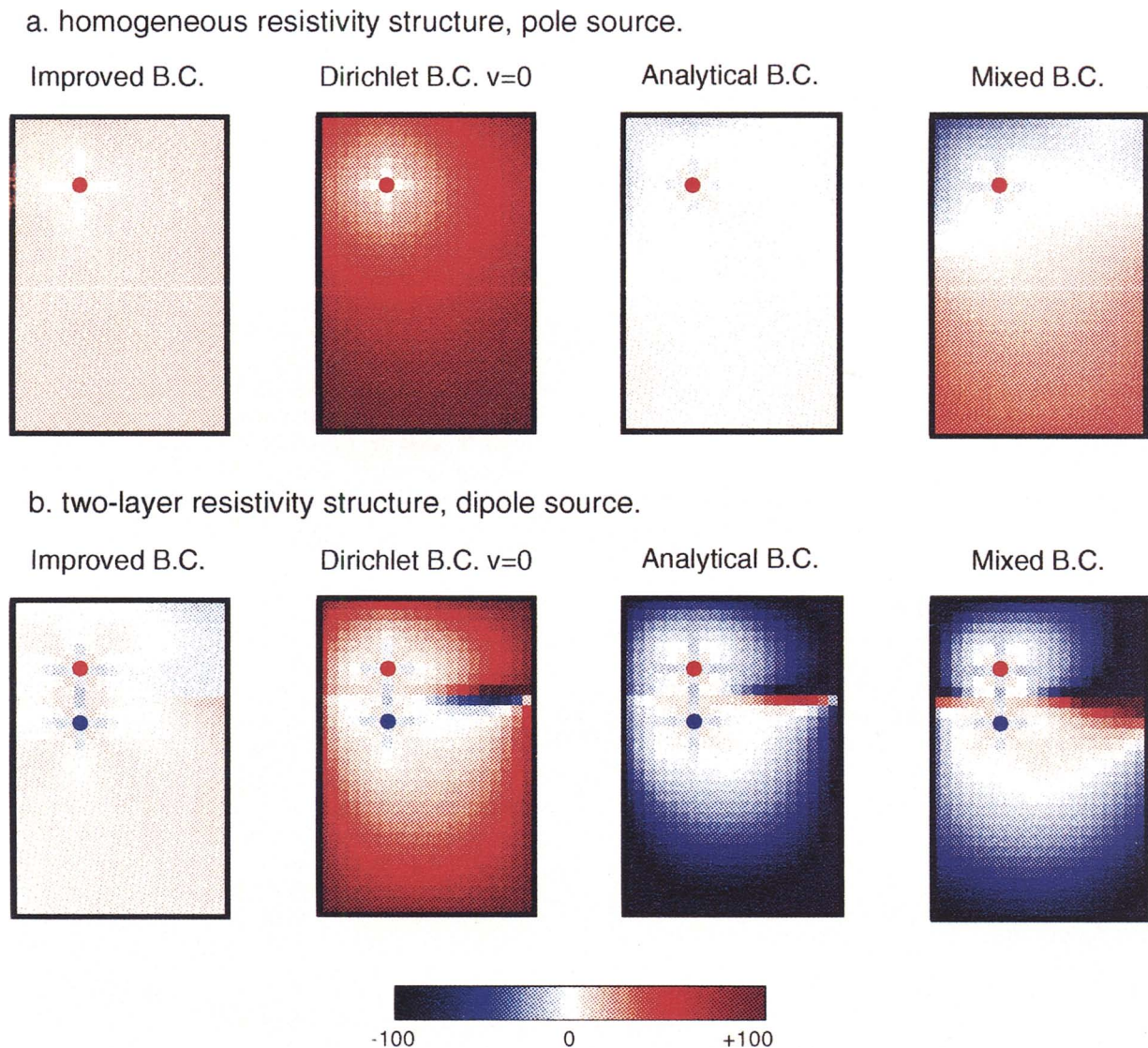

FIG. 2. Forward modeling accuracy in percentage for four different boundary conditions relative to the analytical solutions: (a) pole source, homogeneous resistivity structure, $\rho = 500 \ \Omega \cdot \mathrm{m}$; (b) dipole source, two-layer resistivity structure, $\rho_1 = 500 \ \Omega \cdot \mathrm{m}$, $h = 30$ m, $\rho_2 = 200 \ \Omega \cdot \mathrm{m}$. Equal grid spacing of 10 m was used in these calculations.

dously large because of this boundary condition, and is mostly over 50% on the surface. Another possible boundary condition is to use an analytical solution of the homogeneous medium for the boundary nodes. However, the error for this boundary condition can also be very large if the medium is inhomogeneous and a solution for a homogeneous medium is applied. Consequently, Dey and Morrison (1979) proposed a mixed boundary condition, assuming that the total potential at large distances from the geometrical surface center on the ground has an asymptotic behavior $1/r$, giving,

$$\frac{\partial v}{\partial n} + \frac{v}{r} \cos \theta = 0, \tag{5}$$

where θ is the angle between the radial distance from the geometrical surface center and the outward normal spatial coordinate n on the boundaries. This condition still requires coarse grids near the boundaries, though the accuracy is increased somewhat. However, in solving the inverse problem using conjugate gradient relaxation, we need to be able to compute the forward problem with sources distributed at all the receivers simultaneously and with sources distributed throughout the volume simultaneously (Mackie and Madden, 1993). Therefore, we have modified Dey and Morrison's (1979) boundary condition to account for many sources and exact source locations by considering the local current flow at the boundary nodes as a result of each source. If there are ns sources with sizes I_i ($i = 1, 2, \ldots, ns$) where the potential at a bottom or side boundary node N is v_N ($v_N = \sum_{k=1}^{ns} v_N^{(k)}$) and the potential at the next inner boundary node $N - 1$ is v_{N-1} ($v_{N-1} = \sum_{k=1}^{ns} v_{N-1}^{(k)}$), then we have the following voltage relationship based on Dey and Morrison (1979) because of the ith pole source,

$$v_N^{(i)} = v_{N-1}^{(i)} \left(1 - \frac{\Delta z \cos \theta_i}{r_i}\right) \qquad i = 1, 2, \ldots ns, \tag{6}$$

where r_i is the distance between the boundary node and the source i, θ_i is the angle between the radial distance from the source i and the outward normal spatial coordinate n on the boundaries, Δz is the grid spacing at the bottom boundary and should be replaced by Δx or Δy if the side boundaries are considered. For a homogeneous medium, equation (6) gives an exact boundary relation for one current source if r_i starts from the location of source i rather than the surface center. We make an assumption that the v/I ratio (voltage/source current) normalized by the distance r is constant for each source:

$$\frac{r_1 v_{N-1}^{(1)}}{I_1} = \frac{r_2 v_{N-1}^{(2)}}{I_2} = \cdots = \frac{r_{ns} v_{N-1}^{(ns)}}{I_{ns}} = p. \tag{7}$$

Relationship (7) is exact for a homogeneous medium, and gives an approximation for an inhomogeneous medium. If all the sources are included simultaneously, then by linearity the constant p can be written as

$$p = \frac{v_{N-1}}{\sum\limits_{k=1}^{ns} \left(\dfrac{I_k}{r_k}\right)}. \tag{8}$$

We recognize that the component of the voltage at the node $N - 1$ caused by the ith source from equations (7) and (8) is therefore given by

$$v_{N-1}^{(i)} = \frac{v_{N-1}}{\left(\dfrac{r_i}{I_i}\right) \sum\limits_{k=1}^{ns} \left(\dfrac{I_k}{r_k}\right)}. \tag{9}$$

Substituting this into equation (6) and using $v_N = \sum_{k=1}^{ns} v_N^{(k)}$ and $v_{N-1} = \sum_{k=1}^{ns} v_{N-1}^{(k)}$ leads to the boundary condition that we will apply to a general receiver-source problem,

$$v_N = v_{N-1} \left(1 - \Delta z \sum_{i=1}^{ns} \frac{\cos \theta_i}{r_i^2 \sum\limits_{k=1}^{ns} \left(\dfrac{I_k}{r_k}\right)} \right). \tag{10}$$

To implement the boundary condition [equation (10)] in the network system, we simply scale the near-boundary impedance to control the current across the boundary nodes by the following factor,

$$\phi = \sum_{i=1}^{ns} \frac{\cos \theta_i}{r_i^2 \sum\limits_{k=1}^{ns} \dfrac{I_k}{r_k}}. \tag{11}$$

As shown in Figure 2, for a pole or dipole source, the modified boundary condition [equation (10)] gives small errors everywhere on the surface for homogeneous or two-layer model while the mixed boundary condition in Dey and Morrison (1979) produces a small error only in the central area. For the dipole case, it also shows relatively large errors in the area at equal or nearly equal distances to both poles. This is because the voltage in this area is small, and the error in percentage is therefore quite sensitive and large when the boundary condition is not properly imposed.

Forward modeling solution

In this study, we apply two different techniques to solve the forward matrix problem, equation (4), i.e., the Greenfield algorithm (Swift, 1971) and the conjugate gradient technique (Hestenes and Stiefel, 1952). The Greenfield algorithm is essentially an efficient algorithm for block tridiagonal matrices (Golub and Van Loan, 1990). This algorithm reduces a large matrix problem into many small submatrix problems. In our implementation of the Greenfield algorithm, the submatrix has a dimension of $nx \times nz$. Although the Greenfield algorithm is slower than the conjugate gradient approach, it gives the exact solution of the difference equations whereas the conjugate gradient method gives only an approximate solution. Thus, the Greenfield algorithm is useful for the purpose of checking the modeling accuracy because of boundary conditions and the use of the conjugate gradient method. The numerical calculation shown in Figure 2 used the Greenfield algorithm.

When using the conjugate gradient approach, we need to store only the nonzero elements in the upper triangular part of the symmetric $\underline{K}$ matrix. In the 3-D forward problem, the number of nonzero elements is $7(nx \times ny \times nz) - 2 \times nx$

$\times ny - 2 \times ny \times nz - 2 \times nx \times nz$, but we need to store only $4(nx \times ny \times nz) - nx \times ny - ny \times nz - nx \times nz$ (diagonal + upper triangular) because of symmetry. To represent the sparse matrix $\underline{K}$, we use the row-indexed sparse storage mode (Press et al., 1992), which requires storage of only about two times the number of nonzero matrix elements. Other methods can require as much as three to five times. Efficient algorithms are used to compute $\underline{K}$ multiplying a vector, which is the essential calculation required in the conjugate gradient techniques.

We have also developed efficient algorithms for doing incomplete Cholesky preconditioning that take into account the sparsity of the $\underline{K}$ matrix. Numerical and theoretical studies indicate that the conjugate gradient techniques work best on matrices that are either well conditioned or just have only a few distinct eigenvalues (Golub and Van Loan, 1990). For linear systems of equations, one can precondition the system using methods such as incomplete Cholesky decomposition (Kershaw, 1978; Papadrakakis and Dracopoulos, 1991), incomplete block decomposition, domain decomposition, or polynomial preconditioners [for general review, see Axelsson (1985)]. For the 3-D resistivity problem, we use the incomplete Cholesky factorization based on rejection by position, forcing the preconditioning matrix to have the same sparsity as the forward modeling matrix. Figure 3 shows a comparison of the computation speed for doing one forward modeling problem using the conjugate gradient relaxation with the incomplete Cholesky preconditioning (open circle) versus the Greenfield algorithm (triangle). The grid length refers to the number of grids in each dimension for a cube
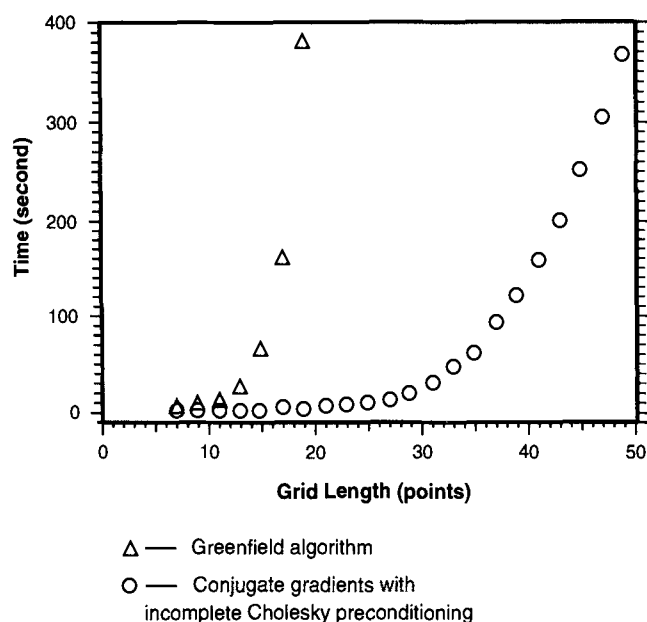

FIG. 3. Computation speed comparison for one forward modeling run using the conjugate gradient techniques with incomplete Cholesky preconditioning (open circle) versus the Greenfield algorithm (triangle). The grid length refers to the number of grids in each dimension for cube models. These calculations were conducted on a Sun SPARCstation 2.

model. These tests were conducted on a Sun SPARCstation 2. We used an accuracy criterion of $|\Delta v/v| < 1e^{-5}$ for these tests. The medium resistivities were completely inhomogeneous and were defined by the function, $\rho(i, j, k) = 100 \times i + 10 \times j + 1 \times k$, so that the speed estimates using the conjugate gradients should represent a lower bound.

MAXIMUM LIKELIHOOD INVERSE PROCEDURE

We apply the maximum likelihood inverse theory developed by Tarantola and Valette (1982) to our 3-D resistivity inversions. In general, geophysical inverse problems are nonunique. The maximum likelihood inverse is one method to obtain a solution to a nonunique inverse problem. This method provides the best fit to the data relative to the a priori information. The mathematical form of the maximum likelihood inverse that we use is from Mackie et al. (1988) and Madden (1990), and it closely follows the work of Tarantola and Valette (1982) and Tarantola (1987):

$$(\underline{A}_k^T \underline{R}_{dd}^{-1} \underline{A}_k + \underline{R}_{mm}^{-1})\Delta m_k = \underline{A}_k^T \underline{R}_{dd}^{-1}(d - \underline{G}(m_k))$$

$$+ \underline{R}_{mm}^{-1}(m_0 - m_k) \qquad (12)$$

where,

$\underline{A}$ = sensitivity matrix
d = observed data vector
m = model vector
$\underline{G}$ = forward modeling operator
$\underline{R}_{dd}$ = data covariance matrix
$\underline{R}_{mm}$ = model covariance matrix
m_0 = a priori model
Δm_k = model changes for inversion iteration k.

For one source, m receivers and n resistivity blocks, the sensitivity matrix $\underline{A}$ is defined by $A_{ij} = \partial Q_i/\partial \rho_j$; $i = 1, 2, \ldots, m$; $j = 1, 2, \ldots, n$, where Q_i is the measurement at the ith receiver and ρ_j is the intrinsic resistivity in the jth model block. For a 3-D problem with many sources, however, the matrix $\underline{A}$ can be very large and have a size equal to (# of sources) × (# of receivers) × (# of medium blocks). Nevertheless, using conjugate gradient relaxation techniques to solve the maximum likelihood equations allows us to bypass the actual computation of the sensitivity matrix $\underline{A}$, or the inversion of the $\underline{A}^T \underline{A}$ term. Indeed, we only need the results of matrix $\underline{A}$ multiplying an arbitrary vector x and $\underline{A}^T$ multiplying an arbitrary vector y. As shown in the algorithm given in the Appendix, these vectors are related to the model residuals or the search directions in the conjugate gradient relaxation and are updated at each relaxation iteration.

For the 3-D magnetotelluric (MT) inversion problem, Mackie and Madden (1993) showed that $\underline{A}$ multiplying a vector could be computed with one forward modeling run with scaled sources distributed throughout the volume. Likewise, they showed that $\underline{A}^T$ multiplying a vector could be computed with another forward modeling run except with scaled sources at the surface. Thus, for each relaxation iteration, only two forward problems are required to compute an update of Δm_k. The total number of forward problems per inversion iteration is determined by the number of relaxation iterations carried out at each inversion iteration. Thus, each inversion iteration required only

2 × *nrel* forward problems, which could be substantially less than doing inversion by traditional methods.

We recognize that we can also compute $\underline{A}$ and $\underline{A}^T$ multiplying arbitrary vectors without forming $\underline{A}$ by using another approach based on reciprocity (Rodi, 1976). There may be situations where this approach may require fewer forward problems than the method in Mackie and Madden (1993). This will be detailed shortly.

To thoroughly investigate each method (Mackie and Madden, 1993; Rodi, 1976), we present two equations for calculating $\underline{A}x$ and $\underline{A}^T y$ that explicitly contain the forward problems required by both Rodi (1976) and Mackie and Madden (1993). In our implementation of the maximum likelihood inverse, we use logarithmic parameterization of the data and model parameters. In all the following equations, however, we keep the sensitivity terms in the original definition, so that the physical meaning can be easily understood. To better illustrate the methods, the following algorithm is developed for a 3-D problem with one source, m receivers and n resistivity blocks. Problems with more sources can be easily modified.

A potential measurement Q_i can be defined as

$$Q_i = a_i^T \boldsymbol{v}, \tag{13}$$

where, $i = 1, 2, \ldots, m$ is the receiver index, $\boldsymbol{v}$ is the voltage vector containing voltage values at all network nodes and for $a_i^T = (0, \ldots, 0, 1, 0, \ldots, 0)$, 1 is the ith component in the vector a_i^T, which corresponds to the receiver site i.

The partial derivative with respect to ρ (medium resistivity) of equation (4) is given by

$$\frac{\partial \underline{K}}{\partial \rho} \boldsymbol{v} + \underline{K} \frac{\partial \boldsymbol{v}}{\partial \rho} = 0. \tag{14}$$

Substituting equation (13) into (14), we get the sensitivity term,

$$\frac{\partial Q_i}{\partial \rho} = -a_i^T \underline{K}^{-1} \frac{\partial \underline{K}}{\partial \rho} \boldsymbol{v}. \tag{15}$$

The matrix $\partial \underline{K}/\partial \rho$ contains only a few terms, which are those associated with the medium ρ in the forward matrix, and it can be analytically derived. The sensitivity matrix $\underline{A}$ multiplying a vector x has the form

$$\underline{A}x = \begin{bmatrix} \dfrac{\partial Q_1}{\partial \rho_1} x_1 + \dfrac{\partial Q_1}{\partial \rho_2} x_2 + \cdots + \dfrac{\partial Q_1}{\partial \rho_n} x_n \\[2mm] \dfrac{\partial Q_2}{\partial \rho_1} x_1 + \dfrac{\partial Q_2}{\partial \rho_2} x_2 + \cdots + \dfrac{\partial Q_2}{\partial \rho_n} x_n \\[2mm] \vdots \\[2mm] \dfrac{\partial Q_m}{\partial \rho_1} x_1 + \dfrac{\partial Q_m}{\partial \rho_2} x_2 + \cdots + \dfrac{\partial Q_m}{\partial \rho_n} x_n \end{bmatrix}$$

$$= - \begin{pmatrix} a_1^T \\ a_2^T \\ \vdots \\ a_m^T \end{pmatrix} \underline{K}^{-1} \left(x_1 \frac{\partial \underline{K}}{\partial \rho_1} \boldsymbol{v} + x_2 \frac{\partial \underline{K}}{\partial \rho_2} \boldsymbol{v} + \cdots + x_n \frac{\partial \underline{K}}{\partial \rho_n} \boldsymbol{v} \right). \tag{16}$$

Similarly, the transposed sensitivity matrix multiplying a vector y is given by,

$$\underline{A}^T y = -(y_1 a_1^T + y_2 a_2^T + \cdots + y_m a_m^T) \underline{K}^{-1} \begin{bmatrix} \dfrac{\partial \underline{K}}{\partial \rho_1} \boldsymbol{v} \\[2mm] \dfrac{\partial \underline{K}}{\partial \rho_2} \boldsymbol{v} \\[2mm] \vdots \\[2mm] \dfrac{\partial \underline{K}}{\partial \rho_n} \boldsymbol{v} \end{bmatrix}. \tag{17}$$

Note that the matrix $\partial \underline{K}/\partial \rho_i$ in these equations contains only a few nonzero terms with algebraic expressions and can be calculated exactly. There are two possible ways to compute $\underline{A}x$ and $\underline{A}^T y$ in equations (16) and (17). First, one can define a vector u for computing equation (16) such that,

$$u = \underline{K}^{-1} \left(x_1 \frac{\partial \underline{K}}{\partial \rho_1} \boldsymbol{v} + x_2 \frac{\partial \underline{K}}{\partial \rho_2} \boldsymbol{v} + \cdots + x_n \frac{\partial \underline{K}}{\partial \rho_n} \boldsymbol{v} \right), \tag{18}$$

and another vector s for computing equation (17) such that

$$s^T = (y_1 a_1^T + y_2 a_2^T + \cdots + y_m a_m^T) \underline{K}^{-1}. \tag{19}$$

Equation (18) can then be rewritten as

$$\underline{K}u = \left(x_1 \frac{\partial \underline{K}}{\partial \rho_1} \boldsymbol{v} + x_2 \frac{\partial \underline{K}}{\partial \rho_2} \boldsymbol{v} + \cdots + x_n \frac{\partial \underline{K}}{\partial \rho_n} \boldsymbol{v} \right). \tag{20}$$

To calculate u, we simply do one forward problem with a source vector $(x_1 \, \partial \underline{K}/\partial \rho_1 \, \boldsymbol{v} + x_2 \, \partial \underline{K}/\partial \rho_2 \, \boldsymbol{v} + \cdots + x_n \, \partial \underline{K}/\partial \rho_n \, \boldsymbol{v})$, in which x_i $(i = 1, 2, \ldots, n)$ is the ith element of the given vector x. The source vector represents the sources distributed throughout the model volume. Likewise, because $\underline{K}$ is symmetric, equation (19) can be rewritten as

$$\underline{K}s = (y_1 a_1^T + y_2 a_2^T + \cdots + y_m a_m^T). \tag{21}$$

The term $(y_1 a_1 + y_2 a_2 + \cdots + y_m a_m)$ represents sources distributed at all receiver sites with source size y_i at receiver i. By doing one forward problem according to equation (21), we can obtain the results of $\underline{A}^T y$. In these two forward problem equations (20) and (21), however, the source sizes are scaled by the vector components of x and y. As mentioned earlier, these vectors need to be updated after each relaxation iteration. Therefore, the total number of

forward problems per inversion iteration by this method is $2 \times nrel$.

The second approach is to solve $\mathbf{u}^T = \mathbf{a}_i^T \underline{\mathbf{K}}^{-1}$, $i = 1$, $2, \ldots, m$, which because of symmetry is equivalent to solving $\underline{\mathbf{K}}\mathbf{u} = \mathbf{a}_i$, $i = 1, 2, \ldots, m$ (Rodi, 1976). These are needed by both equations (16) and (17). This suggests that we need to do m (# of receivers) forward problems with a unit source at one receiver site each time. This idea is similar to Rodi's (1976) algorithm for setting up a sensitivity matrix for the MT problem. However, we bypass dealing with each sensitivity term and directly compute the results of the sensitivity matrix or its transpose multiplying a vector as needed in the conjugate gradient relaxation techniques. Once these calculations are done, then each relaxation iteration requires only updating the appropriate vectors, so no further forward problems are necessary. In essence, since the resistivity problem involves point current sources, we see that by doing forward problems with a current source at each receiver, we have effectively generated the numerical Green's functions.

For each inversion iteration, therefore, we see that when using Mackie and Madden's method (1993) $2 + 2 \times nrel$ forward problems are required including two forward problems needed to update the $\mathbf{b}$ vector before the start of the relaxation loop ($nrel$ is the number of relaxation steps in one inversion iteration). Using the approach based on Rodi (1976), one would need to do $1 + m$ forward problems per inversion iteration (m is the number of receivers). The difference of total computation time between the two methods mostly depends on the number of forward problems required in the inversion procedure. Figure 4 illustrates the difference between the two approaches. For example, with one source and 12 receivers in the field, and three relaxation steps per inversion iteration, this means, by Rodi (1976), $1 + 12 = 13$ forward problems for one inversion iteration; by Mackie and Madden (1993), $2 + 2 \times 3 = 8$ forward problems for one inversion iteration.

However, if we want to take 10 relaxation steps in one inversion iteration for solving the same problem, by Rodi (1976), $1 + 12 = 13$ forward problems for one inversion iteration; by Mackie and Madden (1993), $2 + 2 \times 10 = 22$ forward problems for one inversion iteration.

There is yet an additional way to compute the sensitivity terms. For a network formulation, we can use the Cohn's sensitivity theorem (Tripp et al., 1984), which is efficient when reciprocity is applied. Tripp et al. (1984) solved the 2-D resistivity inverse problem using this approach to explicitly construct the sensitivity matrix. However, Cohn's sensitivity theorem deals with the local current across each network node, so there is a lot of overhead associated with keeping track of the current values across each node. Nevertheless, we have implemented Cohn's sensitivity theorem to provide a cross-check on the other computations.

Figure 5 shows the results of the sensitivity matrix multiplying a unit vector by using three different methods: Cohn's sensitivity theorem (Tripp et al., 1984), the method based on Rodi (1976), and Mackie and Madden's (1993) method. The sensitivity matrix multiplying an unit vector gives the summation of the partial derivatives of each receiver with respect to all medium parameters. This can be understood from equation (16). Clearly, the results from all three meth-

ods are quite comparable to one another, and the differences are minor. The results from Mackie and Madden's (1993) approach and the approach based on Rodi (1976) are almost identical.

Results for synthetic data

Three-dimensional resistivity inversion is very nonunique because there are so many model parameters compared to data points. It is necessary, therefore, to provide constraints to the inversion. Constraints can be applied through the inverse of the model covariance matrix, $\mathbf{R}_{mm}^{-1}$. This matrix is generated prior to the inversion and can be used to weight various model parameters. The model can be smoothed by using off-diagonal terms that couple adjacent parameters. Likewise, the model covariance can be used to correlate model parameters in some predetermined manner, to force certain parameters to have more/less freedom to change
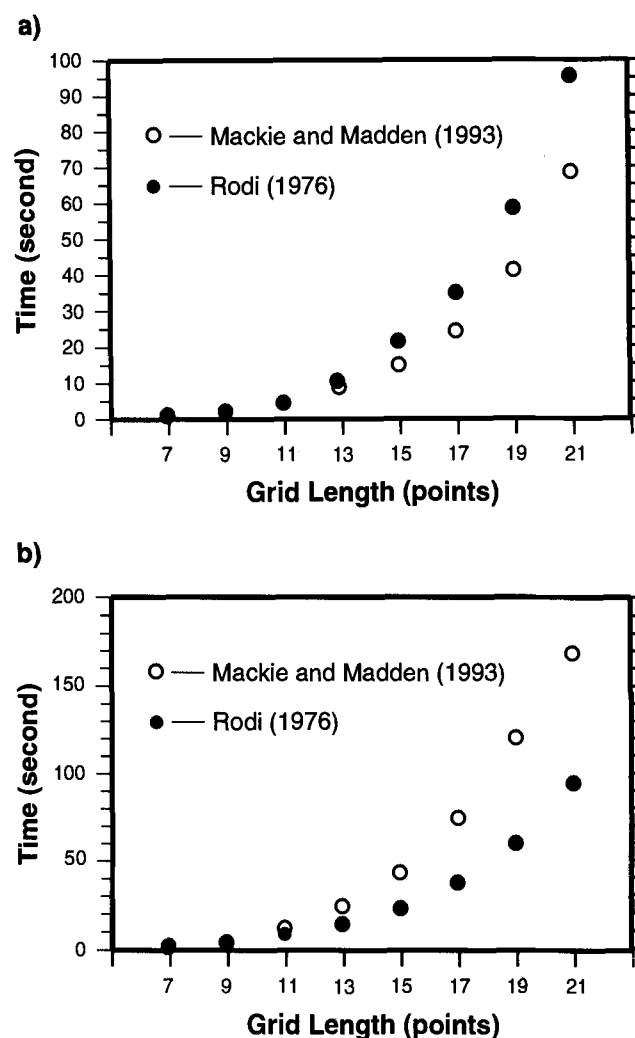
a)

b)

FIG. 4. Comparison of computation speed for one inversion iteration with different relaxation steps by using Mackie and Madden's (1993) method and another approach based on Rodi (1976). The grid length refers to the number of grids in each dimension for cube models. These calculations were conducted on a Sun SPARCstation 2.

during the inversion, or to apply a filter other than near-neighbor smoothing. In our inversion, we also add a variable damping term to the left-hand side of equation (12) to stabilize the inversion in the beginning, and we tie it to the error in the right-hand side so that as the error decreases, so does the added damping. The damping term ε is $\alpha \times (1/\sigma_d^2) \times$ (right-hand side error), where α is an empirical scaling parameter usually on the order 0.1 to 1.0, and the right-hand side is defined as,

$$\sqrt{\frac{\sum\limits_{i=1}^{nmod} b(i)b(i)}{nmod}} \times 100, \qquad (22)$$

where $b(i)$ is the right-hand side vector in equation (12). The damping term reduces the influence of the small eigenvalues in the early stages of the inversion, then allows them to

become more influential at the latter stages. In other words, the use of this damping term maintains a stable convergence rate in the maximum likelihood inverse procedure.

Our numerical simulations have shown an unfortunate result of the nonuniqueness of the resistivity problem and the large sensitivity of the near-electrode model blocks that can duplicate the effects of substantial changes deeper in the model. That is, without additional constraints the inversion tends to make large model resistivity changes in the near-surface layers, and especially in the near-electrode model blocks. This is understandable because a check of the sensitivity terms reveals that the near-electrode model blocks normally have the largest sensitivity. After testing many different inversion constraints, we have settled on the following steps as a reasonable approach: (1) we set the starting resistivity of the shallow layers to an average value determined by the nearest source-receiver combinations, (2)
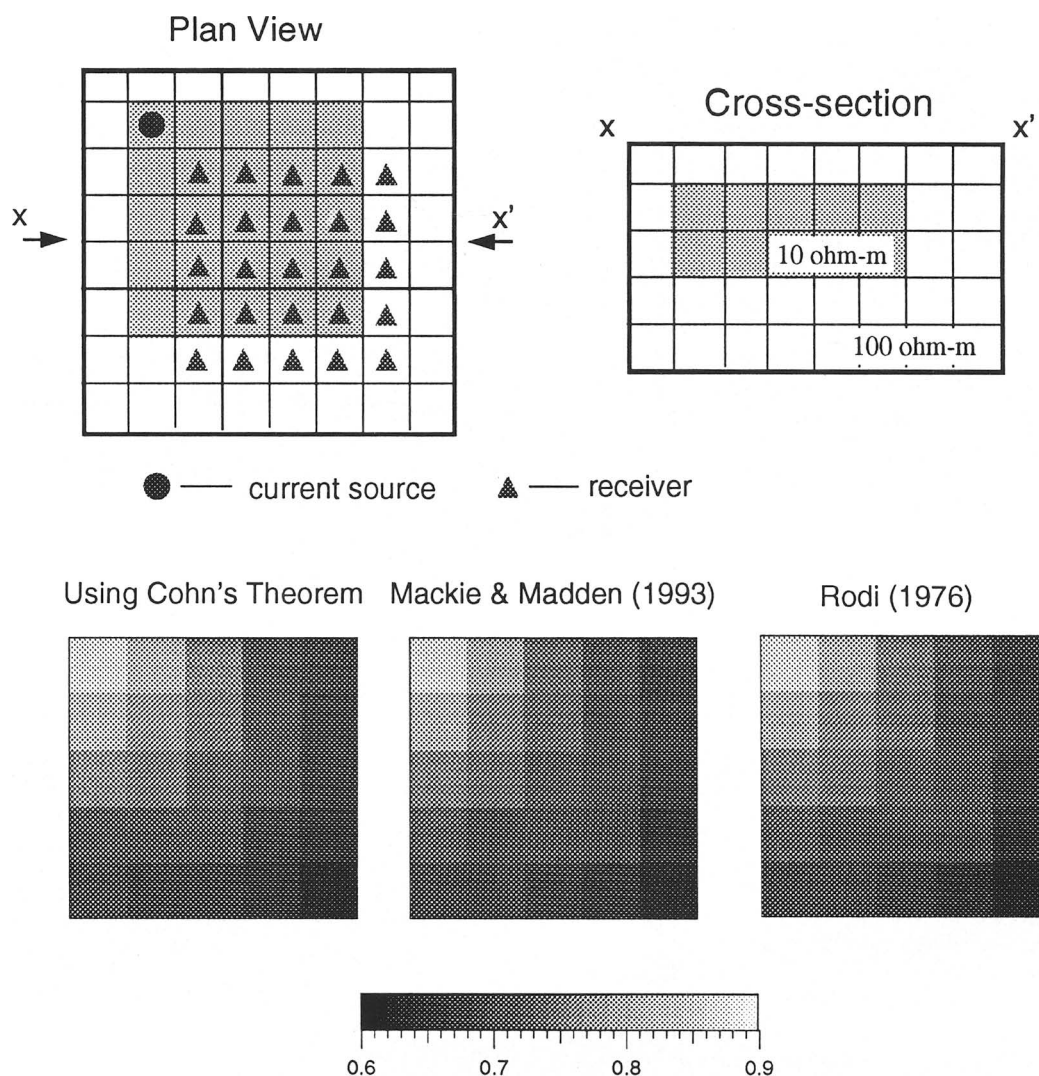

FIG. 5. Results of sensitivity matrix multiplying a unit vector (in natural logarithm) by using three different approaches, Cohn's sensitivity theorem, Mackie and Madden's (1993) approach, and another approach based on Rodi (1976). The model contains a low resistivity zone.

the model covariance is adjusted so that the upper several layers are weighted less than the bottom layers (this means that initially large resistivity changes are not allowed in the shallow structure), and (3) near-neighbor smoothing is also applied. With these constraints, about 10–15 inversion iterations are required to fit the data; however, we obtain much more realistic results than inversions without these constraints.

To demonstrate our 3-D resistivity inversion, we show the results for a pole-pole array with a grid of 5×5 electrodes on the surface and five electrodes in a borehole at one corner (see Figure 6a). The model contains a conductive zone with a resistivity value of 10.0 $(\Omega \cdot m)$ at a depth of 50 m in the background of 100.0 $(\Omega \cdot m)$. The model size is $50 \times 50 \times 20$ with an equal spacing of 6.25 m in all three dimensions. In this numerical experiment, each electrode is used as a transmitter and also as a receiver. Each time one pole transmits current, voltage measurements are taken at all the other poles. Therefore, there are 870 readings that are taken as the data input in the inversion. Figure 6b shows the anomaly sensitivity in percentage for two different sources (circled in Figure 6a): one in borehole, the other on surface. To understand numerical modeling accuracy, noise-free synthetic data are applied.

To calculate synthetic data for M poles, one needs to do M forward problems with a source at each pole. Therefore, we can modify equations (16) and (17) to include M equations in a column or a row for the $\underline{A}x$ and $\underline{A}^T y$ calculations, where $x = (x_1, x_2, \cdots x_n)$ and $y = (y_2^{(1)}, y_3^{(1)} \cdots y_M^{(1)}, y_1^{(2)}, y_3^{(2)}, \cdots y_M^{(2)}, \cdots \cdots y_1^{(M)}, y_2^{(M)}, \cdots y_{(M-1)}^{(M)})$. The vector x still has a dimension of n (the number of model parameters), but the vector y now has a dimension of $M(M - 1)$. Therefore, the $\underline{A}x$ and $\underline{A}^T y$ calculations become $\underline{A}x = (f_1, f_2, \ldots, f_M)^T$ and $\underline{A}^T y = (g_1 + g_2 + \cdots + g_M)$, where f_i and g_i $(i = 1, 2, \ldots, M)$ are given by equations (16) and (17), respectively.
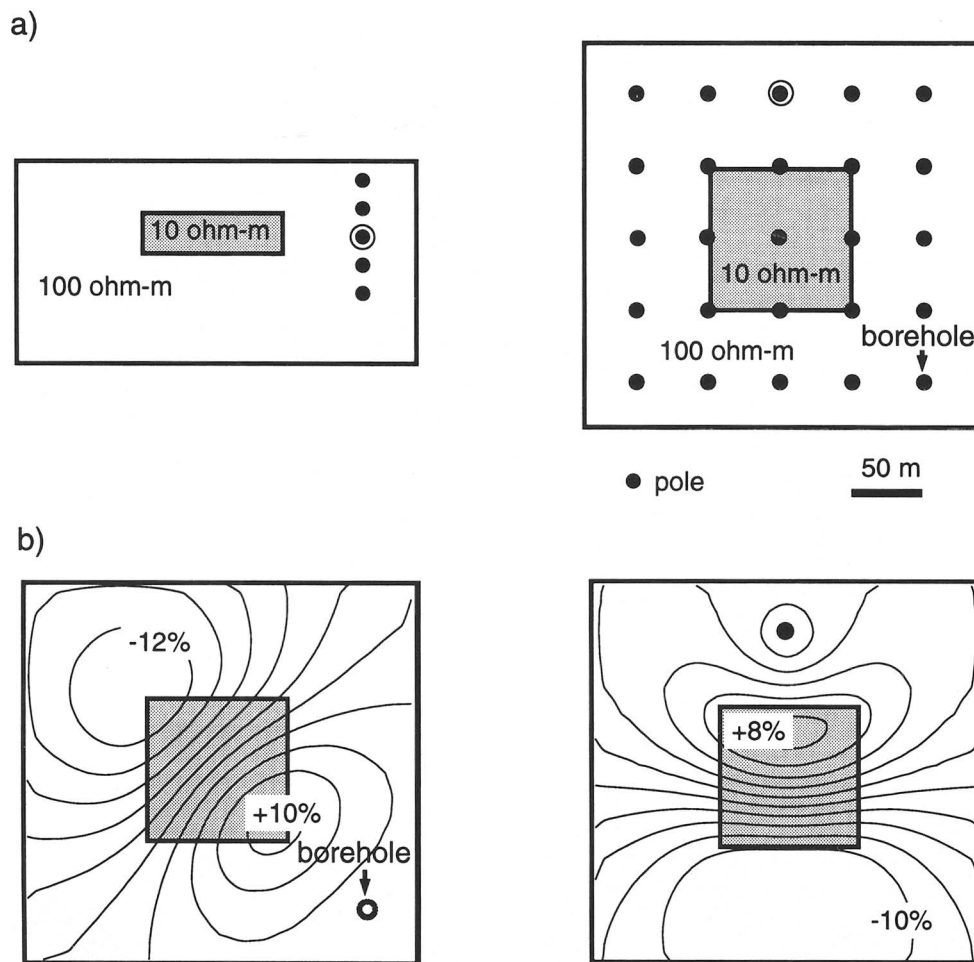
a)

b)

FIG. 6. (a) Cross-section (left) and plan view (right) of the test model. Pole-pole geometry is applied for the numerical test; (b) data sensitivity in percentage because of the conductive zone: one source in borehole (left), the other on surface (right) (circled in Figure 6a).

For a pole-pole problem, since each pole is used both as a receiver and a transmitter and since reciprocity is automatically applied in the field, the results of $a_i^T K^{-1}$ as required in equations (16) and (17) are actually obtained in the initial forward modeling step. Therefore, for this pole-pole problem, we prefer the inversion approach based on Rodi (1976), since no additional forward problems are required for doing the inversion after the initial forward modeling step is completed. For a model size of $50 \times 50 \times 20$ (nx, ny, nz) with 30 poles (870 data readings), one inversion iteration with 10 relaxation steps takes 65 minutes (CPU time) on a Sun SPARCstation 2, and 24 minutes (CPU time) on a DEC alpha workstation.

The conductive zone in Figure 6 comprises $16 \times 16 \times 5$ blocks. For this conductive zone, the largest voltage changes on the surface are about 10%. The lateral changes on the surface are smooth, though some rapid changes occur near the anomaly in the subsurface. This simply suggests that we are not able to resolve the sharp features in the subsurface with any number of receivers on the surface. However, if the receiver spacing is too large, spatial aliasing may become a problem. For this test, we used a grid of 5×5 surface poles with a pole-pole spacing of 50 m, or 8 grids.

As mentioned earlier, a nonuniform weighting of the model covariance is important to the success of resistivity inversion. For this problem, we use a spatial weighting matrix that contains layer weights varying from $1e^{-3}$ to $1e^{-5}$ for the shallow structures of the a priori model, and $1e^{-3}$ for the deep layers, except near the poles in the borehole a larger weighting of $1e^{-3}$ is uniformly applied. The starting model was homogeneous, with a resistivity value of 89.5 $\Omega \cdot m$, which is the average apparent resistivity from the closest pole-pole measurements. This gave an initial 93% rms data fit error. After 10 iterations, the data error was reduced to 2.0%. We stop here for this noise-free synthetic test, because the error in the forward modeling is probably about 2.0 to 3.0%. The results are shown in Figure 7. Clearly, the
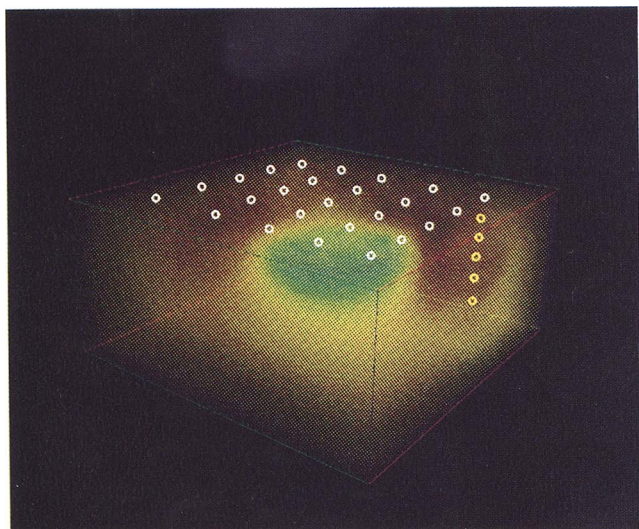
sharp features of the conductive anomaly, such as the corners, cannot be resolved, however, the location, the average size, and the low-resistivity of the zone can be determined from the inversion.

Analysis of field data

At the Mojave Generating Station in Laughlin, Nevada, a resistivity monitoring system was installed beneath and around one of the evaporation ponds operated by Southern California Edison (Van, 1990; Van et al., 1991). This system uses an 8×8 grid of electrodes, with an approximate spacing of 90 m between electrodes. The purpose of this monitoring system is to detect changes in resistivity that would be associated with a leak of saline water from the pond. A sketch map from Van (1990) is given in Figure 8 to show the field layout.

A field test using a scaled down version of the resistivity monitoring system to collect pole-pole data was performed to demonstrate the effectiveness of using this system to detect changes in resistivity associated with the influx of water into the subsurface. The test consisted of a grid of 5×5 electrodes that had exactly the same distance scale and surface pole-pole geometry as shown in Figure 6. A background resistivity survey performed prior to the placement
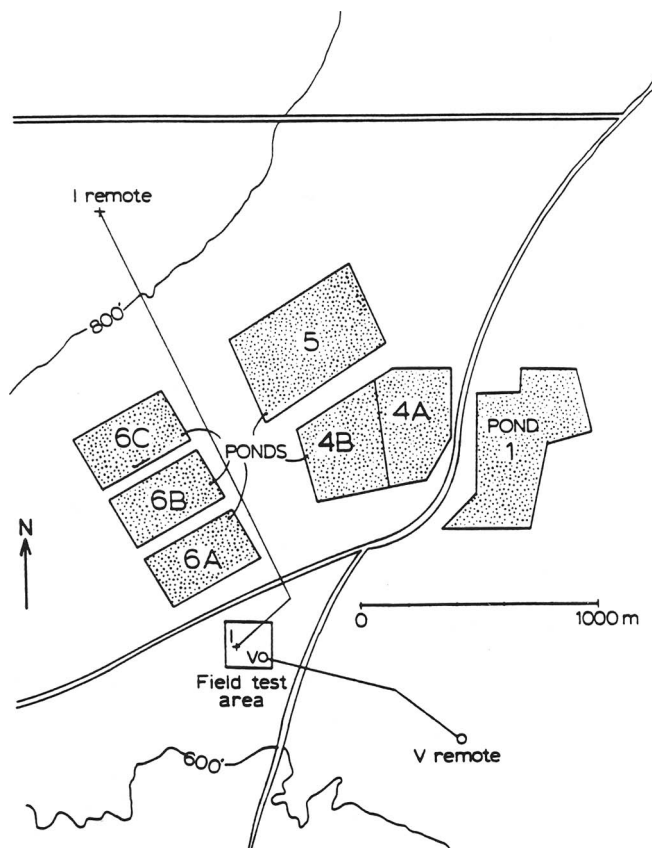

FIG. 7. Inversion results using 25 surface pole-pole data and 5 borehole pole-pole data.

FIG. 8. Map of the field experiment at the Mojave Generating Station in Laughlin, Nevada (from Van, 1990). A grid of 5 × 5 poles using the same surface geometry shown in Figure 6a was used to collect data, no borehole data available in this case.

of water was used as a comparison for the measurements taken afterwards and to determine the resistivity structure of the test area. Park and Van (1991) applied a 3-D inversion algorithm to image the background resistivity structure. However, as a result of the limitation in the algorithm, they could invert only a small number of model parameters (7 × 7 × 5). In this paper, we present the results of modeling the same data but with more efficient forward modeling and inversion techniques and a mesh of 50 × 50 × 20 grids. Another study using the same techniques to model the resistivity monitoring data collected during the experiment is currently being conducted and will be published separately.

Based on pole-pole apparent resistivity analyses, we find that the resistivities in the shallow structures may vary between 400 $\Omega \cdot$ m and 600 $\Omega \cdot$ m. Considering the fact that the apparent resistivities decrease with the increase of pole-pole distance and the water table is at the depth of about 45 m (Park and Van, 1991), we believe this estimate is just a lower bound for the average values from the surface down to 30 or 40 m. The rms data fit error for the inversion starts at 76.0% and drops down to 4.2% after 12 iterations, where we stop the inversion. This is because that analysis of the raw data suggests that 85% of the data satisfies reciprocity with error below 4%. As shown in Figure 9, from the
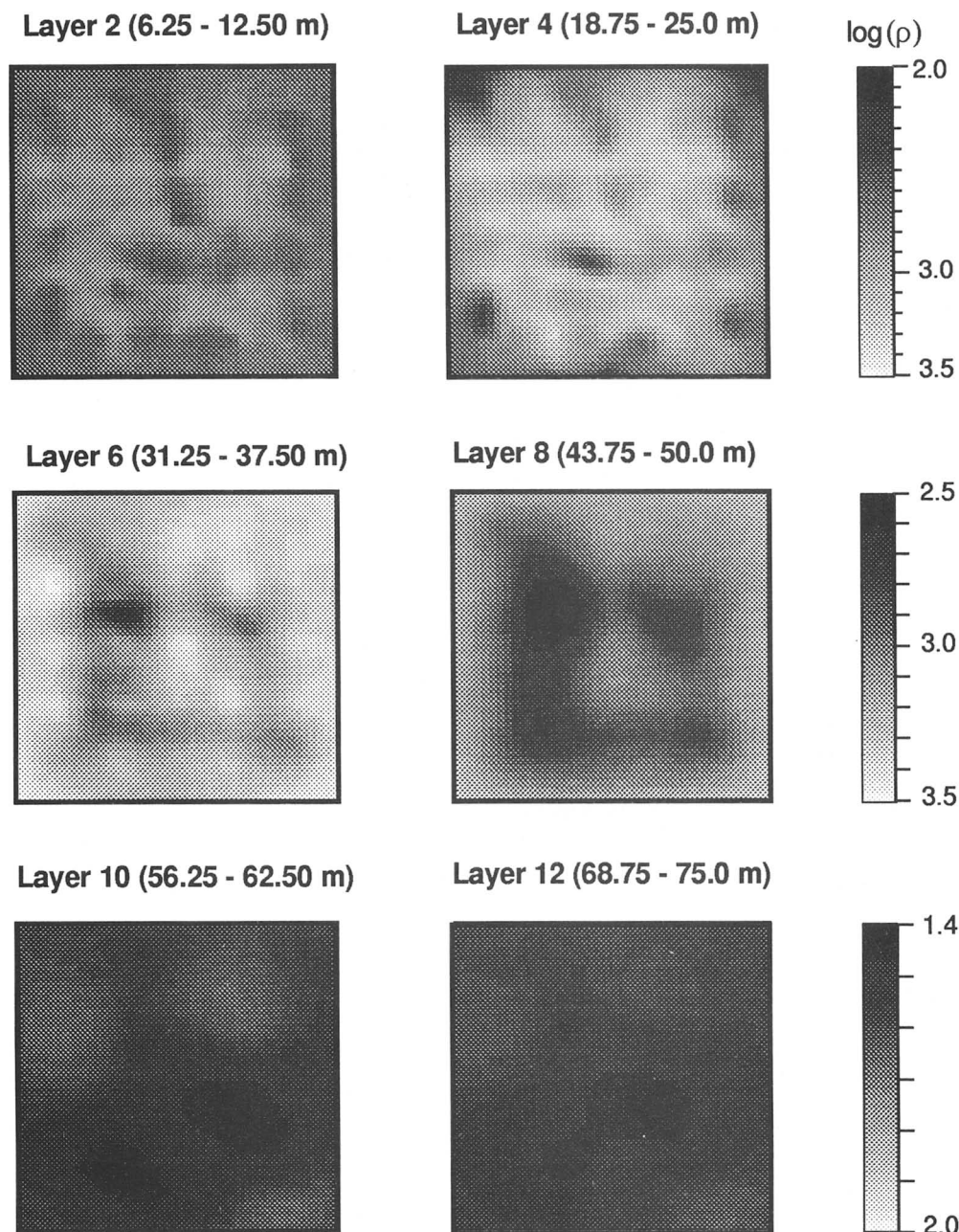

FIG. 9. Six layers of the tomographic imaging results for the baseline survey data collected in Laughlin, Nevada (in logarithm of base 10).

surface down to 25 m, no significant lateral changes are resolved, but changes do occur vertically. In layer 2 (6.25 to 12.50 m), the resistivities vary between 600 and 800 $\Omega \cdot$ m. In layer 4 (18.75 to 25.00 m), however, resistivities vary between 1000 and 2000 $\Omega \cdot$ m. The 3-D variations in the medium become apparent below the depth of 30 m. Between layer 6 and 8, one can see that there is a high resistivity zone (about 2300 $\Omega \cdot$ m) near the center. Because the measurements have low sensitivity to the medium near the boundaries at this depth and the a priori model had high resistivities for these layers, the inversion results show a pattern of high resistivity near the boundaries. This is just an artifact rather than true image. The depth of the water table remains the same as what was given in the a priori model, but also shows slight variations with a 3-D pattern. We have run many inversions with different deep resistivity structures in the a priori model each time, and we are always able to resolve the same features.

The average resistivity in each layer shown in Figure 9 is comparable to that obtained by Park and Van (1991). However, our results more clearly show the lateral and vertical variations that are important for studying leakage monitoring data collected afterwards.

SUMMARY

We have developed rapid 3-D dc resistivity modeling and inversion algorithms using conjugate gradient relaxation methods. We have also modified Dey and Morrison's (1979) mixed boundary condition so that it gives more accurate modeling results. Instead of using only one inversion approach, we have tried to obtain a more thorough understanding of various techniques, and we have analyzed the advantages and disadvantages of each technique for the 3-D problem. The inversion algorithms are presented in a general form, which allows us to use pole-pole data and/or dipole data on the surface and/or in boreholes. We have suggested constraints for minimizing the nonuniqueness of 3-D resistivity inversions based on an appropriate weighting of the model covariance. However, this procedure by no means guarantees a unique solution or a "true" solution. One must combine the results of other geophysical and geological studies to make the interpretation whenever possible.

We believe that the investigation of subsurface features using 3-D resistivity imaging techniques will become an increasingly important exploration tool in the future.

ACKNOWLEDGMENTS

REFERENCES

Axelsson, O., 1985, A survey of preconditioned iterative methods for linear systems of equations: BIT **25**, 166–187.

Coggon, J. H., 1971, Electromagnetic and electrical modeling by the finite-element method: Geophysics, **36**, 132–155.

Dey, A., and Morrison, H. F., 1979, Resistivity modeling for arbitrarily shaped three-dimensional structures: Geophysics, **44**, 753–780.

Ellis, R. G., and Oldenburg, S. W., 1994, The pole-pole 3-D DC-resistivity inverse problem: a conjugate-gradient approach: Geophys. J. Int., **119**, 187–194.

Golub, G. H., and Van Loan, C. F., 1990, Matrix computation: Johns Hopkins University Press.

Hestenes, M. R., and Stiefel, E., 1952, Methods of conjugate gradients for solving linear systems: J. Res. Natl. Bureau Stand., **49**, 409–436.

Hohmann, G. W., 1975, Three-dimensional induced polarization and electromagnetic modeling: Geophysics, **40**, 309–324.

Kershaw, D. S., 1978, The incomplete Cholesky-conjugate gradient method for the iterative solution of systems of linear equations: J. Comput. Phys., **26**, 43–65.

Li, Y., and Oldenburg, D. W., 1994, Inversion of 3-D DC resistivity data using an approximate inverse mapping: Geophys. J. Int., **116**, 527–537.

Mackie, R. L., Bennett, B. R., and Madden, T. R., 1988, Long-period magnetotelluric measurements near the central California coast: A land-locked view of the conductivity structure under the Pacific Ocean: Geophys. J., **95**, 181–194.

Mackie, R. L., and Madden, T. R., 1993, Three-dimensional magnetotelluric inversion using conjugate gradients: Geophys. J. Int., **115**, 215–229.

Madden, T. R., and Swift, C. M., Jr., 1969, Magnetotelluric studies of the electrical conductivity structure of the crust and upper mantle, in the earth's crust and upper mantle (edited by Hart, P. J.): Geophys. Mono. **13**, Am. Geophys. Union, 469–479.

Madden, T. R., 1990, Inversion of low-frequency electromagnetic data, in oceanographic and geophysical tomography: Elsevier Science Publ., 337–408.

Mufti, I., 1976, Finite-difference resistivity modeling for arbitrarily shaped two-dimensional structures: Geophysics, **41**, 62–78.

Park, S. K., and Van, G. P., 1991, Inversion of pole-pole data for 3-D resistivity structure beneath arrays of electrodes: Geophysics, **56**, 951–960.

Papadrakakis, M., and Dracopoulos, M. C., 1991, Improving the efficiency of incomplete Choleski preconditionings: Comm. App. Numer. Methods, **7**, 603–612.

Pelton, W. H., Rijo, L., Swift, C. M., Jr., 1978, Inversion of two-dimensional resistivity and induced-polarization data: Geophysics, **43**, 788–803.

Petrick, W. R., Sill, W. R., and Ward, S. H., 1981, Three-dimensional resistivity inversion using alpha centers: Geophysics, **46**, 1148–1162.

Press, W. H., Teukolsky, S. A., Vetterling, W. T., and Flannery, B. P., 1992, Numerical recipes: Cambridge Univ. Press.

Rodi, W. L., 1976, A technique for improving the accuracy of finite-element solutions for magnetotelluric data: Geophys. J. Roy. Astr. Soc., **44**, 483–506.

Shima, H., 1990, Two-dimensional automatic resistivity inversion technique using alpha centers: Geophysics, **55**, 682–694.

Swift, C. M., Jr., 1971, Theoretical magnetotelluric and Turam response from two-dimensional inhomogeneities: Geophysics, **36**, 38–52.

Tarantola, A., 1987, Inverse problem theory: Method for data fitting and model parameter estimation: Elsevier Science Publ.

Tarantola, A., and Valette, B., 1982, Generalized nonlinear inverse problems solved using the least squares criterion: Rev. Geophys. Space Phys., **20**, 219–232.

Tripp, A. C., Hohmann, G. W., and Swift, C. M., Jr., 1984, Two-dimensional resistivity inversion: Geophysics, **49**, 1708–1717.

Van, G. P., 1990, A field test of a resistivity monitoring system to detect leakage from storage ponds: M.S. Thesis, University of California.

Van, G. P., Park, S. K., and Hamilton, P., 1991, Monitoring leaks from storage ponds using resistivity methods: Geophysics, **56**, 1267–1270.

APPENDIX A

MAXIMUM LIKELIHOOD INVERSE PROCEDURE USING CONJUGATE GRADIENTS

To solve a nonlinear problem, one must update the model in an iterative inversion by providing small local changes $\Delta \mathbf{m}_k$ each time. The model after the kth step is given by

$\mathbf{m}_k = \mathbf{m}_k + \Delta \mathbf{m}_k$. Using conjugate gradient relaxation techniques to solve maximum likelihood inverse problem given by equation (12) in the text, there are two loops involved.

For $k = 1$ to max # inversion iterations   NONLINEAR INVERSION
$\mathbf{G}(m_k)$ response of current model
$\mathbf{d} - \mathbf{G}(\mathbf{m}_k)$ data residuals
$\mathbf{m}_0 - \mathbf{m}_k$ model residuals
$\mathbf{b} = \mathbf{A}^T \mathbf{R}_{dd}^{-1}(\mathbf{d} - \mathbf{G}(\mathbf{m}_k)) + \mathbf{R}_{mm}^{-1}(\mathbf{m}_0 - \mathbf{m}_k)$
   $= \mathbf{A}^T \mathbf{y} + \mathbf{R}_{mm}^{-1}(\mathbf{m}_0 - \mathbf{m}_k)$,   one $\mathbf{A}^T \mathbf{y}$ calculation
   where $\mathbf{y} = \mathbf{R}_{dd}^{-1}(\mathbf{d} - \mathbf{G}(m_k))$
$\Delta \mathbf{m}_k = 0; \mathbf{r}_0 = \mathbf{b}; \mathbf{r}_1 = \mathbf{b};$ initialize conjugate gradients
    For $i = 1$ to max # relaxation steps ($nrel$)   RELAXATION SOLUTION
    $\beta_i = \mathbf{r}_i^T \mathbf{r}_i / \mathbf{r}_{i-1}^T \mathbf{r}_{i-1}$
    $\mathbf{p}_i = \mathbf{r}_{i-1} + \beta_i \mathbf{p}_{i-1}$ ($\mathbf{p}_1 = \mathbf{r}_0$) update search direction
    $\mathbf{B}\mathbf{p}_i = [\mathbf{A}^T \mathbf{R}_{dd}^{-1} \mathbf{A} + \mathbf{R}_{mm}^{-1}]\mathbf{p}_i$
      $= \mathbf{A}^T \mathbf{y} + \mathbf{R}_{mm}^{-1}\mathbf{p}_i$,
      where $\mathbf{y} = \mathbf{R}_{dd}^{-1}\mathbf{A}\mathbf{x}$ and $\mathbf{x} = \mathbf{p}_i$.   one $\mathbf{A}\mathbf{x}$ and one $\mathbf{A}^T \mathbf{y}$ calculations
    $\alpha_i = \mathbf{r}_{i-2}^T \mathbf{r}_{i-1} / \mathbf{p}_i^T \mathbf{B}\mathbf{p}_i$ step length along search direction
    $\Delta \mathbf{m}_k = \Delta \mathbf{m}_k + \alpha_i \mathbf{p}_i$ update model perturbations
    $\mathbf{r}_i = \mathbf{r}_{i-1} - \alpha_i \mathbf{B}\mathbf{p}_i$ update residuals
    end of loop on relaxation steps
$\mathbf{m}_{k+1} = \mathbf{m}_k + \Delta \mathbf{m}_k$ update model parameters
end loop on inversion iterations

We only need the results of $\mathbf{A}$ matrix multiplying an arbitrary vector $\mathbf{x}$ and $\mathbf{A}^T$ multiplying an arbitrary vector $\mathbf{y}$ in this procedure rather than the sensitivity matrix $\mathbf{A}$ or its inversion.